Properties of plasma radiation during discharges with improved confinement on HL-2A Tokamak

Gao Jin-Ming(高金明)†, Liu Yi(刘 仪), Li Wei(李 伟),
Cui Zheng-Ying(崔正英), Zhou Yan(周 艳), Huang Yuan(黄 渊), and Ji Xiao-Quan(季小全)

Southwestern Institute of Physics, Chengdu 610041, *China*

(Received 26 December 2009; revised manuscript received 2 June 2010)

In the recent experiment on the HL-2A tokamak, two types of improved confinement regimes have been achieved in different configurations. One is the improved confinement regime in limiter configuration during electron cyclotron resonant heating (ECRH), characterized by a sharp decrease in H_α emission accompanied by an increase in the total radiation of plasma, the line averaged electron density and the stored energy of plasma. The other is high confinement regime (H-mode) in divertor configuration during a combination of ECRH and Neutral beam injection (NBI) heating, characterized with edge localized modes (ELMs) besides the features mentioned above. The ELMs are found to be localized on the plasma edge ($r/a \geq 0.8$), causing average losses of particles and stored energy in the ranges of about 1–3% and 3–5% respectively during a single ELM event. So far, the ELMs observed in the HL-2A are type III ELMs with low amplitude and high repetition frequency in a range from 200 Hz to 350 Hz. An investigation of the radiated power density profiles shows that radiative cooling effect plays a significant role in the transition back to the L-mode and the triggering of ELM events.

Keywords: improved confinement, edge localized modes, radiative cooling effect
PACC: 5200, 5255G

1. Introduction

Generally, it is observed that the energy confinement time decreases with the increase of auxiliary heating on fusion device, but when sufficient heating power is applied to plasma, the plasma can undergo a transition from the low confinement (L-mode) regime to an improved confinement regime, i.e. H-mode. In H-mode plasma, the energy confinement time is improved by a factor of 2 to 4 over that in the L-mode phase.[1] The H-mode is currently a promising operating regime for a fusion reactor due to its good energy confinement.[1] So far, different kinds of H-modes, such as very high (VH) mode and enhanced D-alpha (EDA) mode, have been observed in many fusion devices, including tokamak and stellarator.[2−6] However, the transition from L-mode to H-mode is not fully understood till now, though it is widely thought that the characteristic enhancement of the confinement arises from a reduced level of fluctuations in the edge region.[1−5,7] It is still an open issue to find the mechanism of L–H transition through the analysis of features in H-mode discharge. Especially, it is important to analyse such characteristics by comparing results obtained in different machines.

Recently experiments with high power auxiliary heating have been carried out in the HL-2A operated in a low plasma parameter regime, and two types of improved confinement regimes have been observed. The first is in the limiter configuration with ECRH heating at about $I_\mathrm{p} \sim 150$ kA, $B_\mathrm{t} \sim 1.3$ T, and $N_\mathrm{e} \sim 1.2 \times 10^{13}/\mathrm{cm}^3$. The second is in the diverter configuration with a combination of ECRH and Neutral beam injection (NBI) heating at about $I_\mathrm{p} \sim 180$ kA, $B_\mathrm{t} \sim 1.4$ T, and $N_\mathrm{e} \sim 2.2 \times 10^{13}/\mathrm{cm}^3$. The plasma parameters of two types of improved confinement regimes are similar, but the latter regime has been identified as being of H-mode by its high H factor (ITER89P) up to 2 and accompanying features in radiation, such as appearance of sharp ELM burst in H_α emission. In this paper, the properties of plasma radiation in both improved confinement regimes are described, especially the role of plasma radiation in the evolution of plasma confinement.

2. Experimental set-up

HL-2A is a medium size tokamak with double null closed divertor. The geometrical parameters of HL-2A are $R = 1.65$ m and $a = 0.4$ m. Typically, it is oper-

†Corresponding author. E-mail: gaojm@swip.ac.cn
© 2010 Chinese Physical Society and IOP Publishing Ltd

ated at toroidal magnetic field $B_t = 2.4$ T and plasma current between 200 and 480 kA.[8] In the present study, HL-2A is run in the low single null closed divertor configuration with a plasma current of about 130–200 kA, toroidal magnetic field of about 1.2–1.5 T and electron density of about $1 - 3 \times 10^{13}$ cm^{-3}.

The main diagnostics involved in this study are four arrays of bolometers with sixteen-chord in each array. Three of them are installed at the plasma main chamber to measure plasma total radiation with a spatial resolution of 25 mm and a time resolution of 50 μs, and the remaining one is installed in the divertor chamber to measure the radiated power from divertor region with a spatial resolution of 10 mm and a time resolution of 20 μs. Eight-chord HCN laser interferometer ($\lambda = 0.337$ mm) for the measurement of electron density in the central region of plasma ($\rho < 0.6$, where ρ is the normalized minor radius) with a spatial resolution of 70 mm. Furthermore, the electron temperature is measured by seven-chord Thomson scattering with a spatial resolution of 30 mm and a time resolution of 100 ms and electron cyclotron emission (ECE) with twenty chords. The evolution of magnetohydrodynamic (MHD) instability can be observed from five arrays of soft x-ray cameras with twenty-line-of-sight in each array, which give a spatial resolution of 25 mm and a time resolution of 10 μs. The H_α emission is measured by five line-of-sight optical telescopes, four of which are located at the middle plane for uniformly looking through the plasma, the remaining one is used to monitor H_α emission of the outer divertor target. The total stored energy of plasma can be measured by diamagnetic loops, then energy confinement time can be calculated from

$$\tau_{\rm E} = \frac{W}{P_{\rm OH} + P_{\rm auxi} - {\rm d}w/{\rm d}t}.$$

3. Properties of plasma radiation during discharges with improved confinement

3.1. In limiter configuration

A typical improved confinement discharge with 0.57 MW ECRH injection for on-axis heating in the limiter configuration is illustrated in Fig. 1. At the initial phase of ECRH injection, the line averaged electron density decreases and the H_α intensity increases sharply because of the event of pump-out.[9] The confinement time of the discharge in L-mode phase is about 10 ms. But at about 390 ms, the line averaged electron density, the stored energy and the total radiation increase abruptly spontaneously, at the same time the H_α intensity declines, which interprets the fact that the recycling of plasma particles decreases since H_α emission comes from neutral hydrogen entering into the plasma as part of recycling process and is a measure of the recycling of hydrogen between the plasma and the surrounding surfaces.[1,10] Then the electron density and the energy confinement time continue to increase and last more than 200 ms, during which the energy confinement time increases by a factor of 1.5 over that in the L-mode phase, characterized by density drop and a degradation in confinement during additional heating as in the case during 310 ms to 380 ms. It suggests that both particle and energy confinements are improved, for there is no additional gas puff. In addition, it shows some perturbations on the signal of plasma radiation power during the improved confinement phase, just like 'dithering' as observed on ASDEX and TCV,[5,10] though the discharge with improved confinement in the limiter configuration on HL-2A is typically quiescent or absent from edge localized modes (ELMs).

The profile of radiated power density related to the discharge of Fig. 1 is given in Fig. 2. The power density in the centre (the hatched region) is lower than that on the edge, and retains this feature for the whole duration of the improved confinement phase. During the improved confinement phase, radiated power density increases sharply and displays the tendency of asymmetrical distribution in the upper part of plasma as shown in Fig. 2(a). The radiated power density rises by a factor of 2 to 3 at $t = 500$ ms as compared with that at $t = 380$ ms, which can be explained by the change of electron density. It could be seen from Fig. 2(b) that there is a sharp change in the electron density profile. The initial peaked density profile changes into a nearly hollow profile, which would causes a strong increase in the edge region and forms a steep gradient in the elctron density. This leads to the strong radiation ($P_{\rm rad} \propto N_{\rm e}$) on the edge of plasma. Therefore, the gradient of the profile of radiation in the edge region increases step by step from 380 ms to 450 ms.

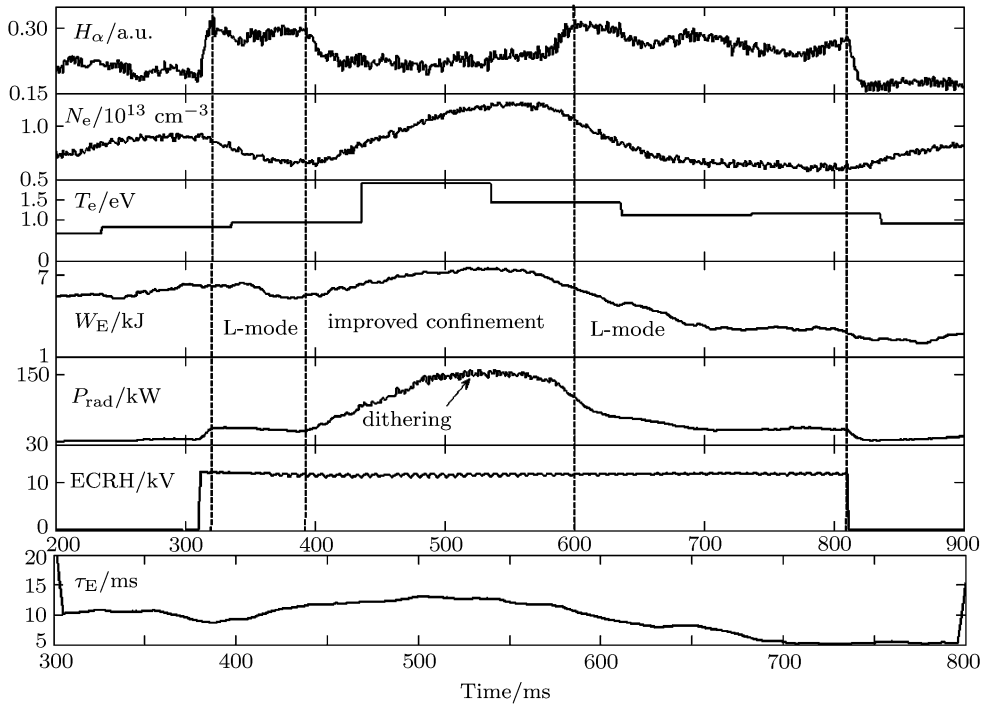


Fig. 1. Time evolutions of H_α emission, line averaged electron density (N_e), electron temperature (T_e), plasma stored energy (W_E), radiated power (P_{rad}), ECRH and energy confinement time (τ_E) for discharge #9548 (I_p = 152 kA, B_t = 1.26 T), (H_α, N_e and T_e are signals that go through the core of plasma), showing that at the beginning of improved confinement H_α emission falls 30% and plasma radiated power increase by a factor of 3.

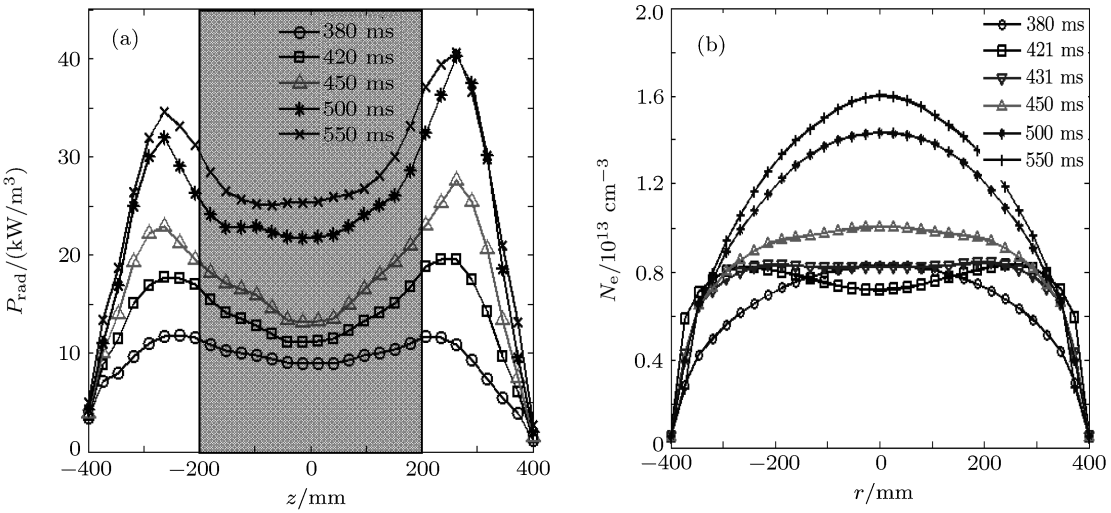


Fig. 2. (a) Profile of plasma radiated powers (after Abel inversion) and (b) the profiles of electron density (after Abel inversion).

Moreover, at the beginning of the improved confinement the electron density profile shows a hollow distribution, but after about $t = 450$ ms, the electron density peaks, thus the radiation further increases, especially in the centre of plasma (the hatched region). At $t = 450$ ms, the radiated power in the hatched region accounts for about 28% of total radiated power, but it rise to 45% of total radiated power at $t = 500$ ms. The increase in radiation is mainly due to the rise in impurity radiation as shown in Fig. 3. Unfortunately, the data of high Z impurity was unavailable on that day, so in order to gain an insight into the process and the effect of impurity radiation in total radiation, the ratio of total radiation to line averaged electron density (P_{rad}/N_e) has been calculated. After the improved confinement transition (indicated by the dashed line), the radiated power is enhanced more rapidly than the increase in density, while after that time, the time trace of P_{rad}/N_e

is approximately flat in the L-mode discharge. This result shows that during the improved confinement phase the impurity confinement is also improved and an additional contribution to total radiation from the enhanced impurity radiation due to improved confinement.[11] The increased impurity radiation along with its cooling effect probably causes a saturation of the energy content of the discharge and a roll-over in plasma confinement, and finally, a forced transition back to the L-mode occurs. Therefore, radiation plays a significant role in the transition from an improved confinement regime achieved in limiter configuration back to the L-mode on HL-2A. Further study will focus on the analysis of the growth of core impurity based on the spectroscopic measurement or the measurement on confinement time of trace impurity by laser blow-off, and also on the extension of the improved confinement regime with silicatization to reduce the content of impurity in HL-2A plasma.

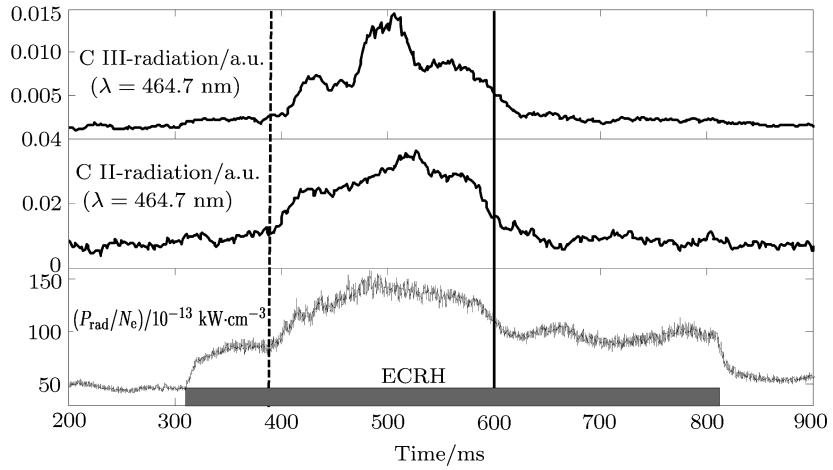


Fig. 3. Time evolutions of CII, C III line radiation intensities and the ratio of $P_{\rm rad}/N_{\rm e}$ for the discharges #9548.

3.2. In divertor configuration

In April 2009, the first transition to H-mode exhibiting improved confinement over that in the L-mode, was achieved on HL-2A in divertor configuration. The profiles of radiated power density in H-mode divertor discharges on HL-2A are similar to those of the improved confinement in limiter configuration in the core of plasma, but characterized by quite different features on the edge of plasma. A typical H-mode discharge in the divertor configuration, with heating by ECRH 0.74 MW and NBI 0.67 MW injected at 487 ms, is displayed in Fig. 4, where time evolution of H_α intensity in the divertor chamber, total radiation, stored energy, line averaged electron density, NBI and the signal of ECRH are shown. The L–H transition is marked by sudden drop (within 2 ms) in the edge H_α emission (proportional to the particle source) and a simultaneous rise in the line-averaged electron density, along with the increase in stored energy and total radiation. In addition, other edge measurements such as edge density and edge temperature measured with a triple probe, consistently show the same tendency. All of these observations are consistent with the transition to the H-phase. It also should be noted that when the additional heating is terminated, the plasma remains in the H-phase for about 6 ms before the density starts to decrease.

Furthermore, regular periodic spikes on the H_α emission are observed during H-mode phase, which are identified as ELMs. It appears as perturbation to the steepened edge density profile as well as radiated power density profile as shown in Fig. 5, where three-dimensional plots of radiated power density and electron density (measured by microwave reflectometry) of H-mode discharge in the outer regions of plasma are given. At L–H transition around 720 ms, the edge density ramps up to about 1.0×10^{13} cm^{-3} and forms a steep density gradient near the last closed surface ($r = 380$ mm). The same tendency appears in the radiated power density distribution. It can be found that the radiated power density increases from 5 kW/m^3 at 400 mm to about 23 kW/m^3 around 380 mm, forming a steep gradient ($\Delta P_{\rm rad}/\Delta r$) of radiated power density of about 900 kW/m^4 on the edge, which is a factor of 3 higher than that of L-mode phase. It can be inferred from the evolution

of the edge density and radiated power density profile that an edge transport barrier is formed on the plasma edge. Typically, such an edge transport barrier is frequently disturbed by the ELM events.

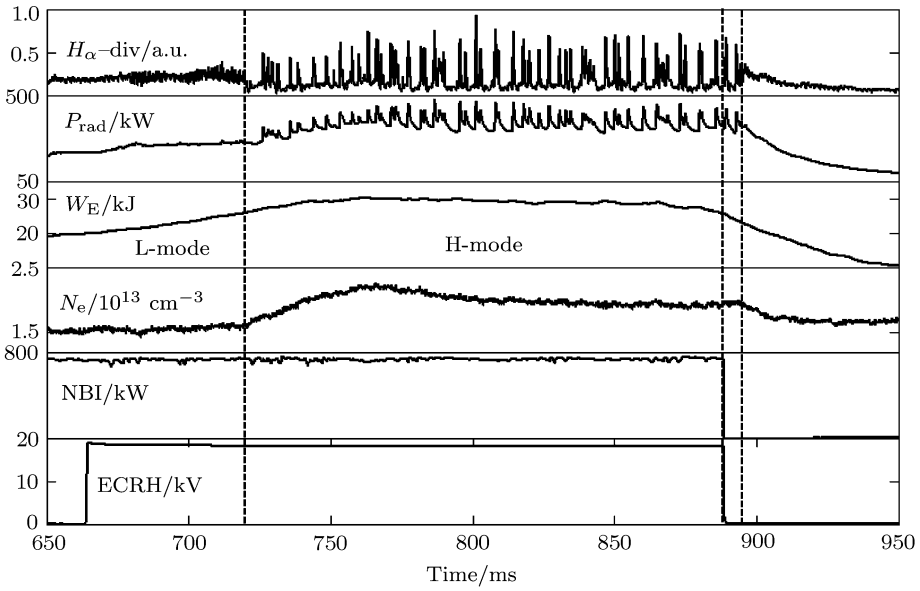


Fig. 4. Time evolutions of H_α emission in the divertor (H_α–div), radiated power (P_{rad}), stored energy (W_E), line averaged electron density of the main plasma (N_e), NBI and ECRH (#11395, $I_p = 176$ kA, $B_t = 1.34$ T) after the L–H transition ELMs are presented. When the additional heating is terminated, the plasma remains in the H-phase for about 6 ms.

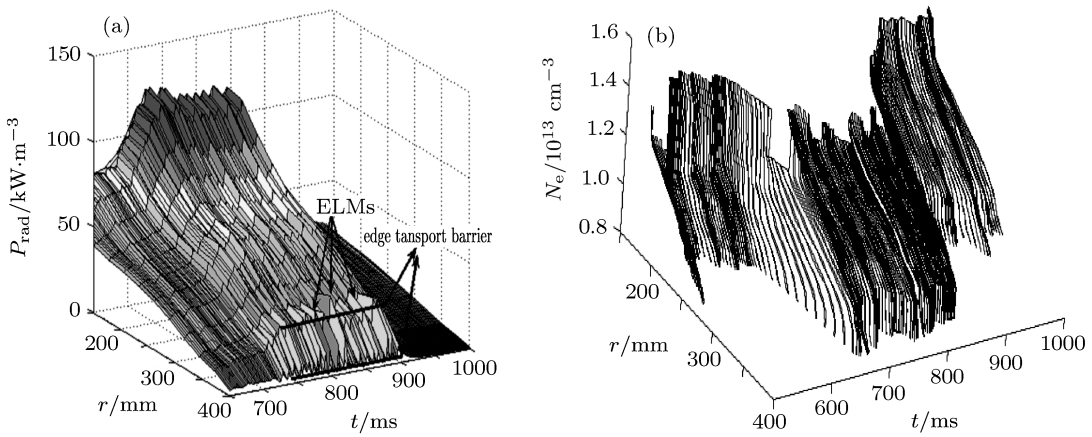


Fig. 5. Three-dimensional plots of radiated power (after Abel inversion) and electron density of H-mode discharge in a range from $r = 150$ mm to $r = 400$ mm, showing the edge transport barrier frequently disturbed by ELMs during H-mode phase.

The ELMs are observed with a low amplitude and high frequency of 200–350 HZ, during which particles and energy are largely lost.[10,12] The losses of particles and stored energy during a single ELM event are about 1–3% and 3–5% compared with those of the total content respectively as shown in Fig. 6. Based on its high frequency range and low average amplitude, and the relatively low resulting losses in plasma particle and stored energy induced by each ELM pulse, the ELMs observed on HL-2A experiments are classified as small ELMs or so called type III ELMs.[10,12]

ELM is a type of MHD instability and usually identified by the characteristic sharp burst of H_α emission arising from the losses of plasma particle and energy,[10] it also manifests itself as a perturbation on the radiation (measured by Bolometer) during H-phase coincident with H_α burst. The profile evolution of radiation during a whole ELM event is shown in Fig. 7(a). The radiated power density profile is hollow with edge lobes covering a quarter of outer plasma range during an ELM event. The radiated power density between 300–400 mm

increases rapidly within 0.3 ms from 491.5 ms to 491.85 ms with the onset of the ELM perturbation, while there is a stagnation point around the 300 mm where nearly no change in radiated power density is observed. This reflects that the ELM itself is localized on the plasma edge ranging from $0.8(r/a)$ to plasma boundary, which is consistent with the presence of a transport barrier just inside the separatrix as indicated on other devices.[1,2,6] Inside the stagnation point, an increase in radiated power is observed in a range from 100 mm to 250 mm, while it decreases inside 100 mm. Then it takes more than 2 ms to go back to the pre-ELM level from 491.85 ms to 493.9 ms. Moreover, in Fig. 7(b) the radial distribution of radiated power fluctuations related to an ELM is shown. It should be noted that the signals of radiation measured by Bolometer are line integral signals, so the signals through the core are affected by the part of the edge, for this reason the above profiles are Abel inverted. On the plasma edge, i.e., $r > 320$ mm, an ELM event causes a transient signal to rise by a factor of 2 to 7 with the increase of relative amplitude, indicating that the ELMs are really 'edge localized' near the plasma edge region from $0.8(r/a)$ to plasma boundary as well as in the inner plasma region from $0.8(r/a)$ up to $0.25(r/a)$, and the influence of ELM event decays to a lower level; more inside, an opposite effect or obvious reduction in the central region is found. Thus, it demonstrates that the increase in radiation intensity on the edge of plasma as observed during ELMs can be ascribed to the particles and energy releasing from the main plasma.

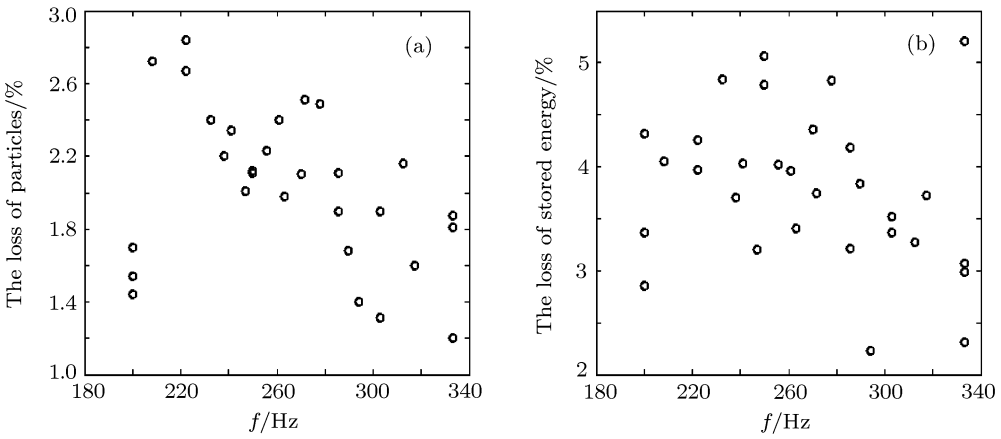


Fig. 6. The losses of particles and stored energy during ELMs versus the frequency of ELMs.

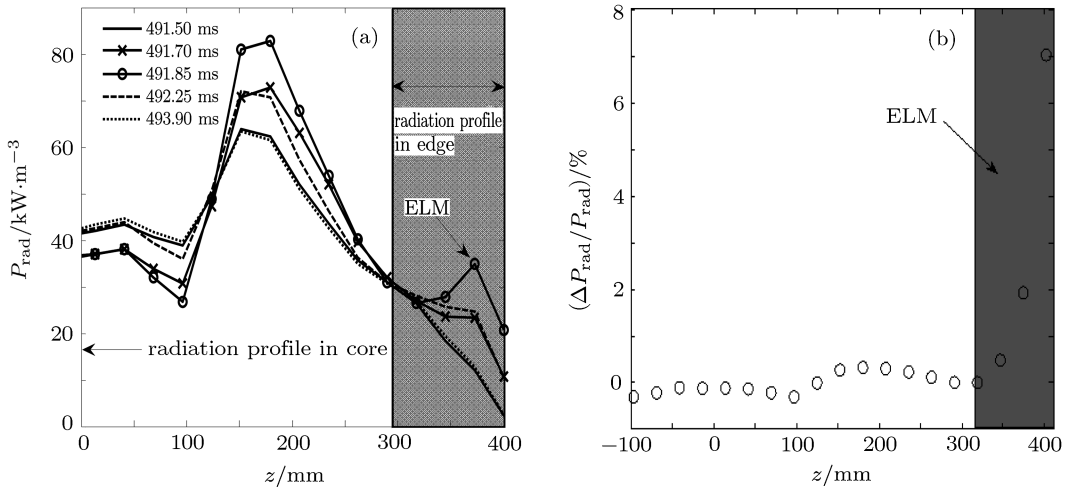


Fig. 7. (a) Profiles of an ELM event based on the data measured by Bolometer(after Abel inversion). During ELMs edge plasma radiation increases from 10 kW/m^3 to 34 kW/m^3 (a factor of 3) within 0.4 ms. (b) Relative variation of plasma radiation due to ELM versus plasma radius.

The total radiation loss during an ELM event is large: its average value is about 300–400 kW, accounting for 30% of total input power as shown in Fig. 8. Usually, ELMs on HL-2A appear erratically and the ELM

period is not well determined and can vary in a certain range for a fixed heating power. Figure 8(a) shows the radiation loss as a function of the time between ELMs (waiting time), while a series of subsequent ELMs with different waiting times are given in Fig. 8(b), showing that the radiated power during an ELM increases with the time between ELMs, implying that more lost power could be caused by an ELM with longer waiting time or lower frequency.

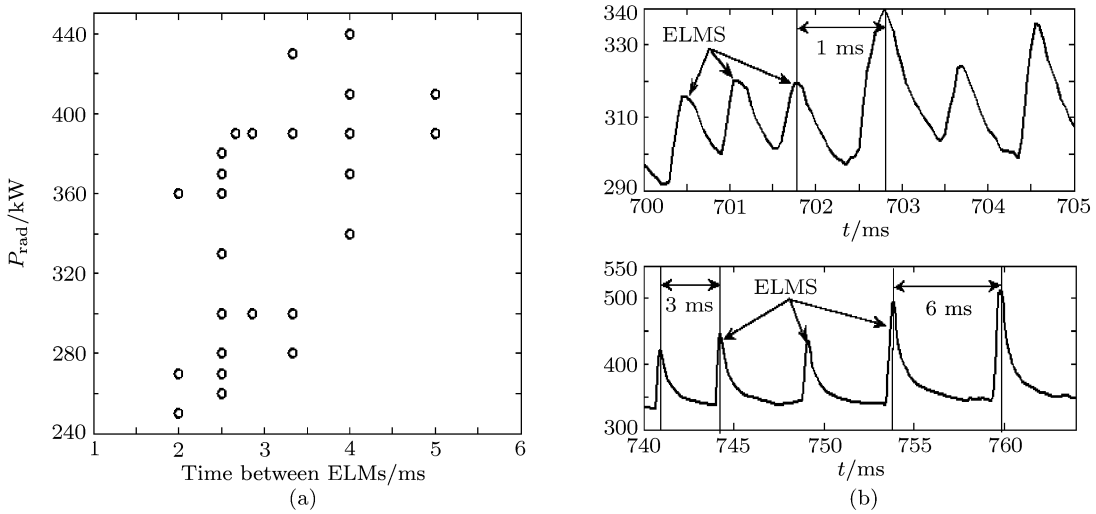


Fig. 8. (a) Radiation loss during an ELM, (b) the time interval between ELMs.

The loss is clearly indicated in Fig. 9, which is a three-dimensional plot of radiated power density at the part of lower plasma density around the divertor during four ELMs and shows sharp increases in radiated power due to particles and energy losses caused by each ELM event. The most of lost energy and particles during ELMs flow into the divertor chamber instantaneously, so there is a burst-like modulation of divertor Bolometer signals as indicated in Fig. 10, which shows H_α emission, radiation from the core, edge and divertor. It can be found in the hatched region that there exist some time delays in the burst of radiation in the divertor chamber with respect to data from the main chamber. The expanded parts of curves on the right-hand side show a delay time of about 200 μs. Such a delay is a consequence of particles flowing across the separatrix at a sound speed from the region of confining plasma to divertor chamber and could provide some useful information about the parallel particle flow and the parallel heat conduction coefficient, which will be described in detail elsewhere.

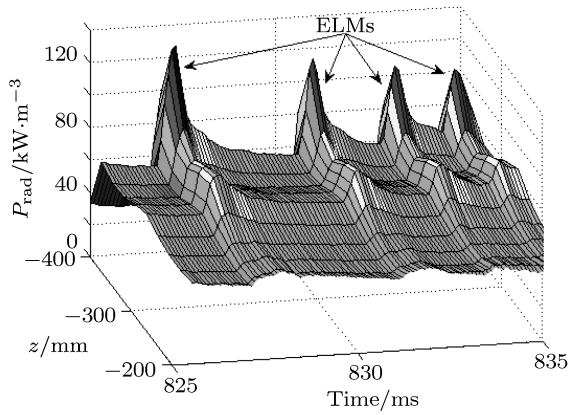


Fig. 9. Three-dimensional plot of plasma radiation over a period of 825–835 ms (after Abel inversion), encompassing four ELMs. During an event of ELM, radiated power increases sharply, thereby interpreting the great losing of particles and energy.

So far, the ELM activity has been taken to be the reason for radiation loss, i.e., the losses of particles and energy, making a degradation to the H-mode confinement. However, along with the losses of particles and energy, ELMs can also eliminate part of impurities, thereby reducing the impurity concentration, which is beneficial to the H-mode confinement. Figure 11 shows that after the L–H transition (indicated by the dash line), the ratio P_{rad}/N_e increases slightly without any sudden increase as shown in limiter improved confinement discharge (Fig. 3). This indicates that the improved confinement in limiter configuration is more susceptible to impurity concentration than H-mode with ELMs in divertor configuration on the HL-2A.

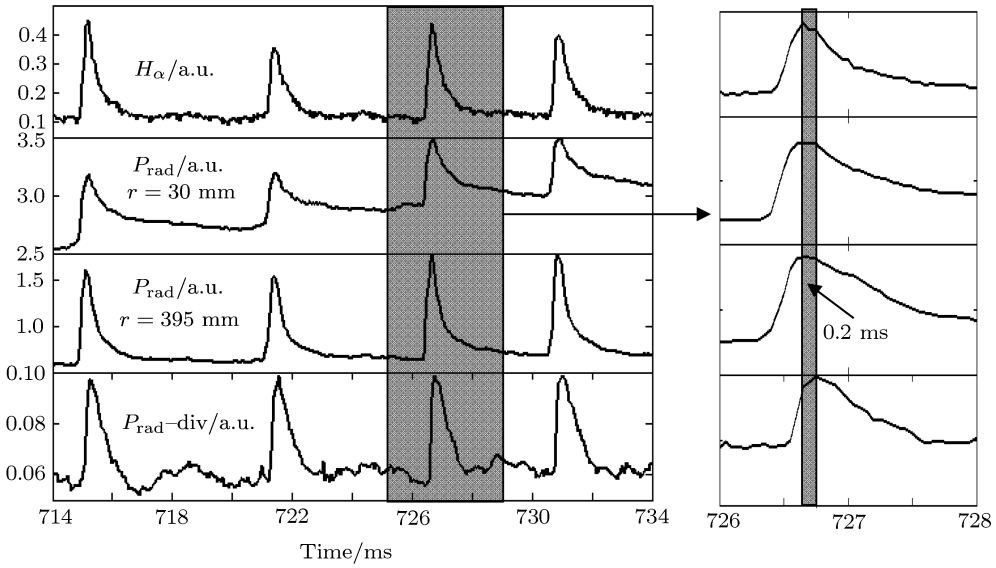


Fig. 10. Data of plasma radiation (meartured by Bolometer) coincident with H_α burst during H-phase. It shoud be noted that the data of plasma radiation in the divertor chamber occur 0.2 ms later than the others due to time delay.

A comparison between Fig. 11 with Fig. 3 shows that according to the L-mode improved confinement, in limiter improved confinement discharge the $P_{\rm rad}/N_{\rm e}$ ratio increases abruptly and displays a tendency of saturation quickly, then goes back to L-mode (indicated by the solid line), but in the H-mode discharge with ELMs in divertor configuration, the $P_{\rm rad}/N_{\rm e}$ ratio increases slightly and does not show the tendency of saturation. Moreover, the H-mode phase is kept till the termination of auxiliary heating. Therefore, ELMs are beneficial to improved confinement to some extent and keep the improved confinement longer.

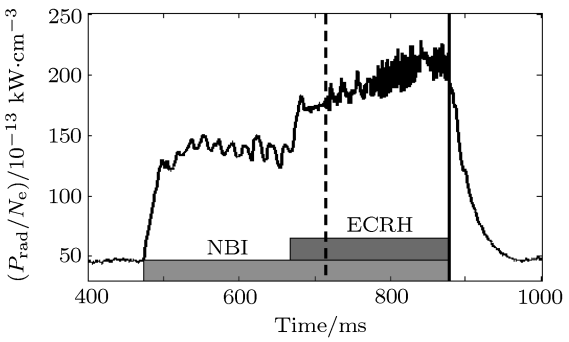


Fig. 11. Ratio of $P_{\rm rad}/N_{\rm e}$ for the H-mode(#11393) discharge.

Analysis of the effect of an ELM event on the radiation can give some valuable information about ELM mechanism. It was found that radiative cooling, which can give rise to improved confinement[13,14] or causes the formation of multifaceted asymmetric radiation from the edge (MARFE),[15] also plays an important role in triggering ELM events. The main impurities in the HL-2A are light impurities such as carbon and oxygen, and their profiles during H-mode, which are as long as profiles during L-mode, are shown in Fig. 12. Figure 13 shows the time evolution of H_α emission, radiation and electron temperature measured with ECE near plasma edge around $r = 300$ mm and Mirnov signal. At about $t_1 = 759.3$ ms, radiation starts to increase. With a delay of about 150 μs, local electron temperature turns to decrease. The power radiated from these impurity species is proportional to the electron density and impurity density and it is also a function of electron temperature. The function of temperature has a principal maximum together with subsidiary maxima at higher temperature. For light impurities the principal maximum occurs at a low temperature according to Ref. [16]. Thus, the radiation from light impurities would rise with the decrease of electron temperature in a range of about tens of eV. Therefore, in the first trace of Fig. 13, the edge plasma radiation loss arising mainly from the incompletely stripped impurities, further increases as electron temperature decreases, thereby leading to a strong cooling effect near the plasma edge. Then at $t_2 = 759.6$ ms the ELM as long as its MHD precursor is triggered as shown in the bottom plot of Fig. 13. This reflects the strong relation to radiation induced cooling effects with the driving of ELM since radiation induced cooling may lead to local change in plasma resistivity and

hence a consequent current profile modification.[17] Therefore, it suggests experimentally that the mechanism of type III ELMs might be related to the change in plasma resistivity due to radiative cooling as suggested in Ref. [17]. This motivates us to search for an alternative way, which is to control ELM activity rather than pellet injection or control coil.[18] This is one of the key issues in plasma research.[19] Specifically, neon or methane, for instance, which is preferentially close to the separatrix, is puffed into plasma to trigger ELM or increase its frequency. Such an experiment is being planned to carry out in our future work.

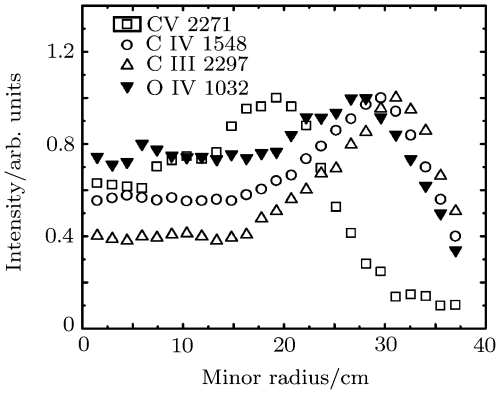


Fig. 12. Normalized impurity emission intensity profiles of C III – C V and O IV.

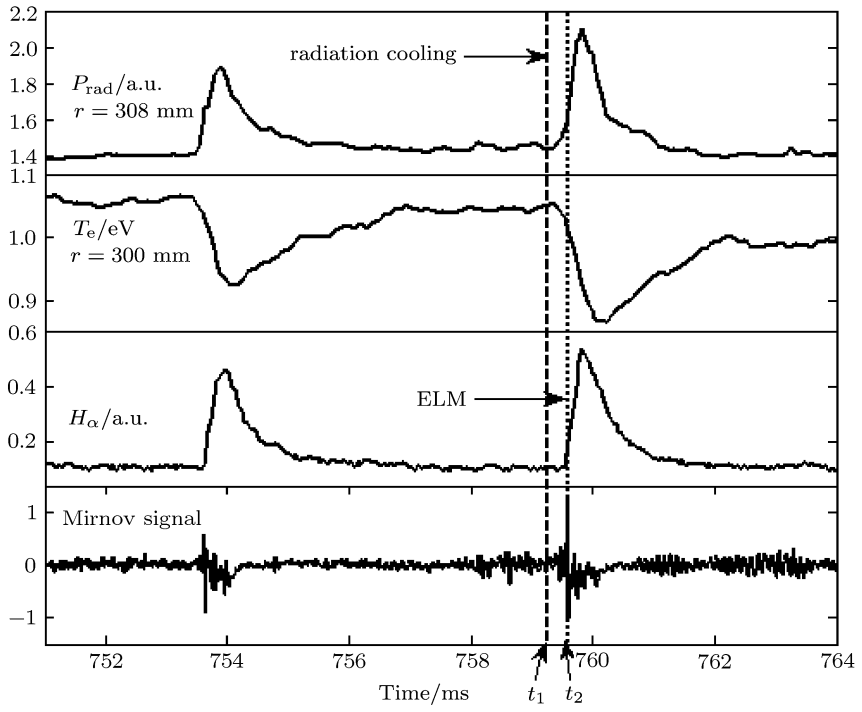


Fig. 13. Time evolutions of H_α emission, plasma radiation, electron temperature and Mirnov signal.

4. Conclusion

Two different improved confinement regimes have been observed under different conditions in the HL-2A. One is in limiter configuration with ECRH heating, characterized by a sharp decrease in the H_α emission and increases in total radiation, line averaged electron density and stored energy. During the improved confinement, the profile of radiated power density shows that radiated power increases sharply and the gradient is steep on the edge of plasma. The other is in divertor configuration with ECRH and NBI heating, characterized by type III ELMs. Analysis shows that ELMs are localized on the plasma edge from $0.8a$ to a, but they can affect plasma in a range from $a/4$ to a. And they can cause energy and particle losses accounting for 3–5% and 1–3% respectively from the main plasma in about 10^{-4} s. A comparison between the two types of improved confinements shows that the improved discharge in limiter configuration is more susceptible to impurity accumulation, and the H-mode with ELMs can relieve impurity accumulation and keep the improved confinement longer. Analysis also shows that radiation loss increases with the time between ELMs, and radiation cooling causes a rapid drop

in the electron temperature, then induces the ELM. However, the driving mechanism of ELMs is still an open issue, although a view universally received is that they are driven by a steep pressure gradient on the edge or a current density profile in a range of the steep electron temperature gradient on the edge.[10] Therefore we will do more work to obtain the abundant data and further carry out investigations to understand the underlying driving mechanism of ELMs.

References

[1] Annette Lindholm Colton 1993 *Experimental Investigation of Edge Localised Modes in JET* Ph.D. dissertation, Roskilde: Risø National Laboratory

[2] Snipes J A, Hubbard A E, Garnier D T, Golovato S N, Granetz R S, Grenwald M, Hutchinson I H, Irby J, LaBombard B, Marmar E S, Niemczewski A, O'Shea P J, Porkolab M, Stek P, Takase Y, Terry J L, Watterson R and Wolfe S M 1996 *Plasma Phys. Control. Fusion* **38** 1127

[3] Filding S J, Ashall J D, Carolan P G, Colton A, Gate D, Hugill J, Morris A W, Valovic M and the COMPASS-D and ECRH teams 1996 *Plasma Phys. Control. Fusion* **38** 1091

[4] Roberts D R, Bravenec R V, Bengtson R D, Brower D L, Cima G, Crowley T P, Darbar A, Edmonds P H, Gasquet H, Gentle K W, Hallock G A, Heard J W, Hurwitz P D, Jiang Y, Karzhavin Y Y, Lierzer J, Nikitin A, Ouroua A, Patterson D M, Phillips P E, Reedy S, Richards B, Rowan W L, Schoch P M, Sing D C, Solano E R, Storek D, Watts C, Winslow D, Wootton A J, Zeng L, Zhang B and Zheng S B 1996 *Plasma Phys. Control. Fusion* **38** 1117

[5] Weisen H, Hofmann F, Dutch M J, Martin Y, Pochelon A, Moret J-M, Duval B P, Hirt A, Lister J B, Nieswand Ch, Pitts R A, Pietrzyk Z A, Anton M, Behn R, Besson G, Buhlmann F, Chavan R, Fasel D, Favre A, Franke S, Isoz P, Lavanchy P, Joye B, Llobet X, Mandrin P, Marletaz B, Marmillod Ph, Magnin J C, Mayor J-M, Paris P J, Perez A, Sauter O, van Toledo W, Tonetti G, Tran M Q, Troyon F and Ward D J 1996 *Plasma Phys. Control. Fusion* **38** 1137

[6] John Lohr, Stallard B W, Prater R, Snider R T, Burrell K H, Groebner R J, Hill D N, Kyoko Matsuda, Moeller C P, Petrie T W, John H St and Taylor T S 1988 *Phys. Rev. Lett.* **60** 2630

[7] Sato M, Fukuda T, Takizuka T, Kamada Y, Tsuchiya K, Shirai H, Ishida S and Mori M 1996 *Plasma Phys. Control. Fusion* **38** 1283

[8] Hong W Y, Yan L W, Qian J, Pan Y D, Wang E Y, Luo C W, Xu Z Y, Pan L, Li Q, Yuan B S, Liu L and Ding X T 2006 *Chin. Phys.* **15** 556

[9] Erckmann V and Gasparino U. 1994 *Plasma Phys. Control. Fusion* **36** 1869

[10] ASDEX Team 1989 *Nuclear Fusion* **29** 1959

[11] Cui Z Y, Zhou Y, Li W, Feng B B, Sun P, Dong C F, Liu Y, Hong W Y, Yang Q W, Ding X T and Duan X R 2009 *Chin. Phys.* B **18** 3473

[12] Connor J W 1998 *Plasma Phys. Control. Fusion* **40** 531

[13] Tsuji S, Hosogane N, Itami K, Kubo H, Nishitani T, Shimada M, Koide Y, Nishino N, Sugie T, Nagashima K, Kawano Y, Naito O, Nakamura H, Yoshida H, Miya N and Nagami M 1992 *Nuclear Fusion* **32** 1313

[14] Hobirk J, Messiaen A M, Finke K H, Ongena J, Brix M, Jaspers R, Koslowski H R, Kramer Flecken A, Mank G, Rapp J, Telesca G and Unterberg B 2000 *Nuclear Fusion* **40** 1469

[15] Zagorski R and Gerhauser H 2004 *Physica Scripta* **70** 173

[16] John Wesson 2004 Tokamaks(THIRD EDITION) (OXFORD: Clarendon Press) p229-231

[17] Zohm H 1996 *Plasma Phys. Control. Fusion* **38** 105

[18] Saibene G, Horton L D, Sartori R, Balet B, Clement S, Conway G D, Cordey J G, De Esch H P L, Ingesson L C, Lingertat J, Monk R D, Parail V V, Smith R J, Taroni A, Thomsen K and von Hellermann M G 1999 *Nucl. Fusion* **39** 1133

[19] Becoulet M, Nardon E, Huysmans G, Zwingmann W, Thomas P, Lipa M, Moyer R, Evans T, Chuyanov V, Gribov Y, Polevoi A, Vayakis G, Federici G, Saibene G, Portone A, Loarte A, Doeber C, Gimblett C, Hastie J and Parail V 2008 *Nucl. Fusion* **48** 024003